2021 IEEE International Conference on Robotics and Automation (ICRA 2021)
May 31 - June 4, 2021, Xi'an, China

IMU/Vehicle Calibration and Integrated Localization for Autonomous Driving

Zhenbo Liu, Leijie Wang, Feng Wen, and Hongbo Zhang

Abstract— **The localization system, which outputs vehicle position, velocity, and attitude, is one of the fundamental components in the autonomous driving vehicle. The global pose is not only used for the planning and control system, but also an important reference for the cloud source-based HD Map building and updating. The accuracy, availability, and reliability are key requirements for the localization system to ensure that the whole system runs smoothly and efficiently.**

IMU/Vehicle extrinsic calibration is one of the primary jobs that should be addressed. Due to the observability issue, the IMU/vehicle relative roll cannot be calibrated by the traditional maneuver-based calibration method. In this paper, we solve this issue with the proposed Multiple Orientation-based Vehicle/IMU Extrinsic Calibration (MOVIE-Cali) method, which is evaluated by Monte Carlo simulations and experiments.

When the vehicle is cornering or making a U-turn, the sideslip of the tires will have negative influence on the localization system which uses Non-Holonomic Constraints (NHC)/Wheel speed sensor measurement in the model. We derive a sideslip angle model and propose an online slip parameter calibration and compensation method to improve the localization accuracy. The performance of proposed method has been evaluated by the vehicle tests.

I. INTRODUCTION

In the autonomous driving, the sensor calibration and localization module are the fundamental components. The intrinsic and extrinsic parameters of the onboard sensors (such as the camera, radars, Inertial Measurement Unit (IMU), LiDAR, wheel speed sensor (WSS), and GNSS antenna) need to be calibrated and used by different subsystems. For example, the moving objects tracking module should know the relative pose between each local coordinate systems of cameras, radars, and LiDAR sensors. For the localization system, the relative pose between IMU-frame and vehicle-frame needs to be calibrated to provide the vehicle's global localization and orientation as the input to the planning and control module. On the other hand, the IMU/vehicle extrinsic calibration can be a bridge when the relative pose between IMU and other sensors, given that their extrinsic parameters with respect to the vehicle frame have been calibrated. This is often the practical requirement in the onboard cloud-sourcing mapping system, because the global pose are primarily from the inertial navigation system or integrated navigation system, while the mapping sensors are LiDAR and cameras.

For the localization system, the three "pillars" that define its performance in the autonomous driving application, are accuracy, availability, and reliability. Although GNSS with Real-time kinematic (RTK) corrections plays very important role for the high accuracy (e.g., centimeter-level) global positioning, it cannot work well in scenarios such as tunnels, road under the overpass, city canyons, underground, etc, and maybe jammed or spoofed [1]. Map matching with detailed LiDAR feature maps or vector maps using LiDAR or camera sensors are the alternate solutions to provide the global position [2]–[4]. Due to dynamic object obstruction and bad weather conditions, the performance can be degraded. How to improve the localization accuracy during the global position gaps needs to be studied.

There have been some great works in the LiDAR-camera calibration [5]–[7], IMU-camera calibration [8]–[10], and IMU-LiDAR calibration [11] in the robotics and computer vision community. For the IMU intrinsic calibration, the axis-to-axis misalignments of the gyroscope sensor or accelerometer sensors in the IMU can be calibrated using turn tables or multi-position calibration method [12], [13]. For the IMU-vehicle calibration, most of the works estimate the relative pose parameter in the Kalman filter-based framework with maneuvers [14]–[17]. However, these approach can only calibrate the relative pitch and yaw, because the relative roll is not observable in the state space. [18] assumed the vehicle travels on a horizontal plane and calculate the relative roll angle directly from INS output. This may introduce large errors as the road plane may not be horizontal. To reduce the real-time positioning error during global localization aiding gaps, usually NHC/WSS observations are used in the INS system [15], [16], [19]. The sideslip of the vehicle can cause the violation of the zero lateral velocity in NHC. IMU yaw rate was used for detecting the NHC violation in [20]. [14] used additional vehicle yaw rate and G-sensor to estimate the slip angle for better usage of NHC. [21] provided the method to estimate vehicle sideslip with INS and GPS with one or two antennas, which is not applicable during GPS outages. [22] gave a comprehensive review on the vehicle sideslip angle estimation concentrating on the slip at the gravity centre, not rear axle centre, which is the interested point for NHC in the localization applications.

In this paper, we propose a IMU/vehicle relative attitude calibration method based on multiple vehicle orientations, which can effectively estimate the relative roll angle. The detailed derivation of the method is presented in Section II. To improve the localization performance during global position outages, we present an online sideslip parameter calibration and integration method in Section III and Section IV. Vehicle tests have been performed to show the effectiveness

*This work was not supported by any organization

Zhenbo Liu, Leijie Wang, Feng Wen, and Hongbo Zhang are with Noah's Ark Lab, Huawei, 100085 Beijing, China liuzhenbo3@huawei.com

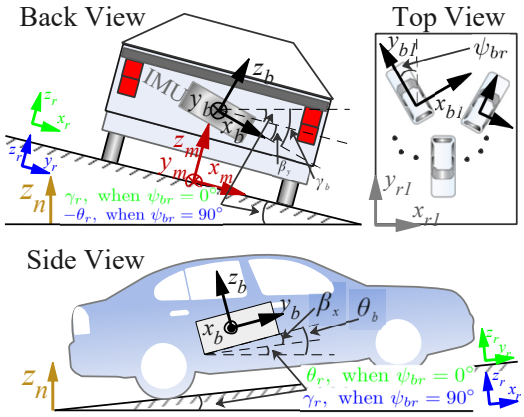

Fig. 1. Coordinate systems and relative angles among them

of proposed methods.

II. Multiple Orientation-based Vehicle/IMU Extrinsic Calibration

The relative roll between IMU-frame and Vehicle-frame is not observable in the tradition INS/WSS/NHC integration. Here we develop an offline IMU-vehicle roll/pitch calibration method. The relative pitch angle estimation can be thought of as a by-product, which is a source for the checker in the calibration process.

A. Relationship among IMU-Vehicle Misalignment, IMU Attitude, and Road Attitude

As shown in Fig. 1, the vehicle frame, denoted by m-frame, is rigidly fixed to the vehicle with the origin being the ground projection of the midpoint of the rear axle. The x_m axis points to the right of the vehicle, the y_m axis points forward, and the z_m axis points upward, based on the right-hand rule. The IMU body frame, denoted by b-frame, originates at the sensitive center of the IMU. To make it coincide with the vehicle frame, axes of b-frame point right, forward, and upward, respectively. The road frame, denoted by r-frame, is attached onto the local road plane. The navigation frame, denoted by n-frame, is the local level frame. In this section, the y_n axis points the same direction with y_r of the first stationary position.

The direction cosine matrix relationship among the frames can be expressed as follows:

$$\boldsymbol{C}_n^b = \boldsymbol{C}_m^b \boldsymbol{C}_r^m \boldsymbol{C}_n^r \tag{1}$$

Decomposing the rotation matrix in Eq.(1) into the product of three Euler angle-based sub-rotation matrices with rotation order of $z-x-y$ (the Euler angle in the parentheses is the related rotation angle), we get

$$\begin{aligned}\boldsymbol{C}_{b_2}^b(\gamma_b)\boldsymbol{C}_{b_1}^{b_2}(\theta_b)\boldsymbol{C}_n^{b_1}(\psi_b) = \boldsymbol{C}_{b_{m2}}^b(\beta_y)\boldsymbol{C}_{b_{m1}}^{b_{m2}}(\beta_x)\boldsymbol{C}_m^{b_{m1}}(\beta_z)\\ \boldsymbol{C}_r^m \cdot \boldsymbol{C}_{r_2}^r(\gamma_r)\boldsymbol{C}_{r_1}^{r_2}(\theta_r)\boldsymbol{C}_n^{r_1}(\psi_r)\end{aligned} \tag{2}$$

where $\beta_i,\ i \in \{x, y, z\}$, is the IMU/Vehicle misalignment. θ_i, γ_i, and ψ_i, $i \in \{b, r\}$ are absolute pitch, roll, and heading of i-frame. Post-multiplying $C_{b_1}^n$, there is

$$\begin{aligned}\boldsymbol{C}_{b_2}^b(\gamma_b)\boldsymbol{C}_{b_1}^{b_2}(\theta_b) = \boldsymbol{C}_{b_{m2}}^b(\beta_y)\boldsymbol{C}_{b_{m1}}^{b_{m2}}(\beta_x) \cdot \boldsymbol{C}_r^{b_{m1}} \cdot\\ \boldsymbol{C}_{r_2}^r(\gamma_r)\boldsymbol{C}_{r_1}^{r_2}(\theta_r)\boldsymbol{C}_{b_1}^{r_1}\end{aligned} \tag{3}$$

Note that the b_1-frame and r_1-frame are the horizontal frames, so $\boldsymbol{C}_{b_1}^{r_1}$ can be described by a single rotation angle (notated as ψ_{br}). The xy-plane of b_{m1}-frame is the same with that of r-frame, so that $\boldsymbol{C}_r^{b_{m1}}$ can also be described by a single rotation angle (notated as ψ'_{br}). Assuming the slope and banking angles of the road surface are normal (not too large), ψ_{br} and ψ'_{br} can be considered equal.

When the road banking or slope angles are not small, a general constraint model derived from Eq. (3) is

$$\begin{aligned}&\sin(\gamma_r)\cos(\theta_r)\sin(\psi_{br}) + \cos(\psi_{br})\sin(\theta_r)\\ &= \cos(\beta_x)\sin(\theta_b) - \cos(\gamma_b - \beta_y)\cos(\theta_b)\sin(\beta_x)\end{aligned} \tag{4}$$

$$\begin{aligned}&-\sin(\gamma_r)\cos(\theta_r)\cos(\psi_{br}) + \sin(\psi_{br})\sin(\theta_r)\\ &= -\sin(\gamma_b - \beta_y)\cos(\theta_b)\end{aligned} \tag{5}$$

When the road bank and slope angles and IMU-vehicle misalignment are small, the following equations are derived, relating the INS pitch/roll angles, IMU-vehicle misalignments, and road slope/banking angles and INS heading w.r.t. road-frame.

$$\begin{cases}\theta_b = \beta_x + \cos(\psi_{br})\theta_r + \sin(\psi_{br})\gamma_r\\ \gamma_b = \beta_y - \sin(\psi_{br})\theta_r + \cos(\psi_{br})\gamma_r\end{cases} \tag{6}$$

B. IMU-Vehicle Roll/Pitch Calibration

Now we describe the offline IMU-Vehicle roll/pitch calibration method based on Eq.(6). For a certain estimation problem, we denote an estimate by $\hat{\bullet}$, and the measurement by $\tilde{\bullet}$. The absolute pitch and roll of INS can be calculated using the accelerometers' output of the IMU when the vehicle is stationary.

$$\tilde{\theta}_b = \arcsin\frac{\bar{f}_y - \hat{b}_{a_y}}{g_0} \tag{7}$$

$$\tilde{\gamma}_b = -\arcsin\frac{\bar{f}_x - \hat{b}_{a_x}}{g_0\cos\tilde{\theta}_b} \tag{8}$$

where g_0 is the local gravity. $\bar{f}_i$ $(i = x, y)$ is the averaged specific forces from accelerometers of i-axis, and $\hat{b}_{a_i}$ is the corresponding pre-estimated bias.

In Eq.(6), there are 4 unknowns, namely, β_x, β_y, θ_r, and γ_r. For each stationary interval, there are two equations. Therefore, at least 2 stationary intervals with different relative yaw of b-frame w.r.t r-frame (i.e., ψ_{br}) are required. It should be noted that the vehicle should be on the same flat ground surface to ensure that the road banking and slope angles (θ_r and γ_r) are constant.

The simplest way for the calibration estimation, which we call "2-Orientation" method, is to obtain 2 stationary with 2 opposite vehicle headings, i.e., $\psi_{br}^{(0)} = 0$ and $\psi_{br}^{(1)} = \pi$. The IMU-Vehicle relative pitch and roll are estimated as

$$\hat{\beta}_x = \frac{\tilde{\theta}_b^{(0)} + \tilde{\theta}_b^{(1)}}{2},\quad \hat{\beta}_y = \frac{\tilde{\gamma}_b^{(0)} + \tilde{\gamma}_b^{(1)}}{2} \tag{9}$$

For generality, the following "multi-orientation" method is to combine multiple stationary data with different vehicle heading directions to obtain more robust calibration result. The different orientations ψ_{br} can be obtained from marked directions on the ground, towards which the vehicle should point. Alternatively, for an easier calibration procedure, ψ_{br} can be calculated by integrating IMU yaw rate ω_z between two stationary intervals, i.e.,

$$\psi_{br}^{(k)} = \psi_{br}^{(k-1)} + \sum_{i=1}^{n_k} \omega_z^{(i)} \Delta t_i \tag{10}$$

where n_k is the number of angular rate frames between the $k-1$-th and k-th stationary intervals. Δt_i is the IMU period.

The state vector here is denoted by $\boldsymbol{x}$.

$$\boldsymbol{x} = \begin{bmatrix} \beta_x, & \beta_y, & \theta_r, & \gamma_r \end{bmatrix}^\top \tag{11}$$

The i-th observation for the i-th stationary interval:

$$\begin{aligned} \boldsymbol{z}_i = \begin{bmatrix} \tilde{\theta_b} \\ \tilde{\gamma_b} \end{bmatrix} &= \begin{bmatrix} 1 & 0 & \cos(\psi_{br}^{(i)}) & \sin(\psi_{br}^{(i)}) \\ 0 & 1 & -\sin(\psi_{br}^{(i)}) & \cos(\psi_{br}^{(i)}) \end{bmatrix} \boldsymbol{x} + \boldsymbol{n}_b \\ &\triangleq \boldsymbol{H}_i X + \boldsymbol{n}_b \end{aligned} \tag{12}$$

where n_b is the measurement noise.

Recursive least square estimator (LSE) is applied to estimate the IMU/Vehicle relative pitch and roll angles, as well as the road pitch and roll angles.

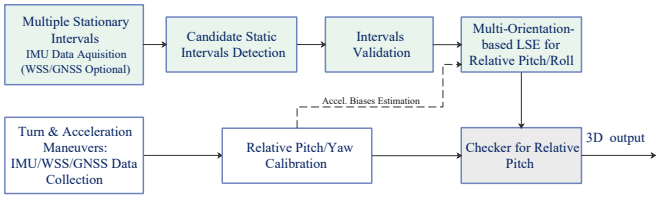

Fig. 2. 3D Boresight Calibration Process

C. IMU-Vehicle 3D Attitude Calibration Process

As the tradition maneuver-based method [16] can only calibrate relative pitch and yaw, we combine the proposed Roll/Pitch calibration together with traditional method to obtain 3D relative attitude.

The whole calibration process is depicted in Fig. 2. Firstly, the vehicle performs the turn and acceleration maneuvers for the pitch/yaw calibration (which is actually the integrated method with online calibration function described in Section IV). The accelerometers' biases can also be estimated in this procedure.

Then the vehicle is required to collect multiple stationary data with different vehicle orientations on the same plane. The static detection algorithm can be used for candidate static datasets formulation, which contains the timestamps, IMU measurements, and calculated IMU absolute horizontal attitude. The continuous vehicle orientation with timestamp is calculated and recorded. The candidate intervals are validated by the criteria of minimum interval length (e.g., 60s, to smooth out the noise), the vehicle's minimum relative orientation among intervals (e.g., 30°, to avoid rank deficiency in LSE), and the maximum position change among intervals (e.g., 4m, to ensure the local flatness). If the number of valid intervals meets the requirement, relative pitch and roll can be estimated using the method in Section II-B. The common parameter, relative pitch, can be examined to check the validness of the calibration process.

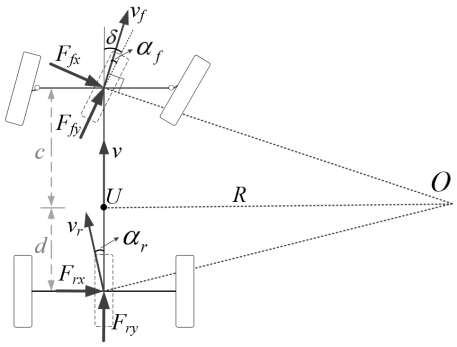

Fig. 3. Bicycle model with sideslip (The turn radius is R.)

III. Sideslip Modeling

A. Sideslip Phenomenon and Modeling

When the vehicle moves normally along a straight line, the moving direction is coincide with four tyre planes. When the tyres experience a lateral force, caused by a turn, lateral wind, etc., a reaction called Cornering Force in the touch area of the tyre exists resisting the lateral movement [21].

The bicycle model considering sideslip is illustrated in Fig. 3. The lateral dynamic equation is:

$$\Sigma F_x = F_{fx}\cos(\delta) + F_{fy}\sin(\delta) + F_{rx} = ma_x \tag{13}$$

Yaw moment equilibrium equation:

$$F_{rx}d - F_{fx}\cos(\delta)c - F_{fy}\sin(\delta)c = 0 \tag{14}$$

where a_x is the lateral acceleration, F_f and F_r are lateral forces on front and rear tyres. δ is the steering angle of front tyres. From Eq. (13) and (14), we have

$$F_{rx} = \frac{cma_x}{l} \tag{15}$$

For small slip angle, the lateral force F_{rx} can be approximated by a linear relationship to the slip angle α_r, with slope being the normalized lateral slip stiffness or the normalized cornering stiffness.

$$F_{rx} = C_\alpha \alpha_r \tag{16}$$

where C_α is the sideslip stiffness, which depends on the tyre type, load, pressure, and so on.

Now we derive the sideslip angle

$$d = R\tan(\alpha_r) \tag{17}$$

$$c = R\tan(\delta_f - \alpha_f) = l - d \tag{18}$$

From Eq.(15), (16), (17) and (18), we have

$$\frac{m(L - R\tan(\alpha_r))}{l} a_x = C_\alpha \alpha_r \tag{19}$$

Suppose the sideslip angle α_r is a small angle, there is

$$\alpha_r = \frac{mla_x}{lC_\alpha + mRa_x} = \frac{mla_x}{lC_\alpha + mv^2} = \frac{1}{\frac{C_\alpha}{m} + \frac{v^2}{l}} a_x \quad (20)$$

To Simplify the model, Eq.(20) is written as

$$\alpha_r = Sa_x \quad (21)$$

where S is a near-constant scale, which is estimated online.

Note that we assume the vehicle does not lose the road grip. Therefore, the range for sideslip angle in this model is within $\pm 2^\circ$ under normal circumstances [23].

IV. Sensor Fusion with Online Slip Estimation and Compensation

The INS-based integrated navigation system, with global position/heading aiding observations (e.g., GNSS, LiDAR map-matching, and Vision map-matching), has been proven to be the robust and continuous onboard localization solution. Here we refine the lateral constraint in NHC virtual observations to account for the sideslip in the rear axle to improve the localization performance during turns.

A. System Model

We use the error-state Kalman Filter architecture. The state vector consists of the errors of velocity, attitude, position, gyroscope biases, accelerometer biases, IMU/Vehicle relative pitch/yaw, scale factor of the wheel speed, and slip parameter.

$$\boldsymbol{X} = \begin{bmatrix} \delta \boldsymbol{v}^{n\top} & \boldsymbol{\phi}^{n\top} & \delta \boldsymbol{p}^\top & \delta \boldsymbol{b}_g^\top & \delta \boldsymbol{b}_a^\top & \begin{bmatrix} \delta\beta_x \\ \delta\beta_z \\ \delta K_{od} \end{bmatrix}^\top & \delta S \end{bmatrix}^\top \quad (22)$$

For detailed INS mechanization, error-state dynamic model, and observability analysis, please refer to [24], [25].

B. Measurement Model

The measurement residual vector is

$$\begin{aligned} \boldsymbol{Z} &= \hat{\boldsymbol{v}}^m_{\text{veh}} - \tilde{\boldsymbol{v}}^m_{\text{veh}} \\ &= \hat{\boldsymbol{C}}^m_b \left(\hat{\boldsymbol{C}}^b_n \hat{\boldsymbol{v}}^n_{\text{ins}} + \hat{\boldsymbol{\omega}}^b_{eb} \times \hat{\boldsymbol{r}}^b \right) - \tilde{\boldsymbol{v}}^m_{\text{veh}} \end{aligned} \quad (23)$$

where $\hat{\boldsymbol{v}}^n_{\text{ins}}$ and $\hat{\boldsymbol{C}}^b_n$ are INS velocity and attitude matrix. $\hat{\boldsymbol{C}}^m_b$ is the IMU/Vehicle relative orientation (e.g., its initial guess can be set identity matrix if the axes of b-frame and m-frame are nearly pointing to the same direction). $\hat{\omega}^b_{eb}$ is the angular velocity of the body frame w.r.t Earth frame. $\hat{r}^b$ is the lever-arm from b-frame to m-frame, which is calibrated by hand or from a total station. The WSS and NHC measurement considering the slip angle is

$$\tilde{\boldsymbol{v}}^m_{\text{veh}} = \begin{bmatrix} \tilde{v}_r \sin(\hat{\alpha}_r) \\ \hat{K}_{od} \tilde{v}_r \cos(\hat{\alpha}_r) \\ 0 \end{bmatrix} \quad (24)$$

where $\tilde{v}_r$ is the measured velocity of the rear wheels.

The design matrix is

$$\boldsymbol{H} = \begin{bmatrix} \boldsymbol{C}^m_n & -\boldsymbol{C}^m_n [\hat{\boldsymbol{v}}^n_{\text{ins}} \times] & \boldsymbol{O}_{3\times 9} & \tilde{v}_r \boldsymbol{M}_1 & a_x \tilde{v}_r \boldsymbol{M}_2 \end{bmatrix} \quad (25)$$

where $\boldsymbol{M}_1 = \begin{bmatrix} 0 & -1 & 0 \\ 0 & 0 & -1 \\ 1 & 0 & 0 \end{bmatrix}$ and $\boldsymbol{M}_2 = \begin{bmatrix} \cos(\hat{\alpha}_r) \\ -\sin(\hat{\alpha}_r) \\ 0 \end{bmatrix}$. The lateral acceleration can be computed by $a_x = \tilde{v}_r \omega_z$.

V. Experiment Evaluation and Analysis

We have tested the multi-orientation calibration method both in the simulation and in the experiment. The integrated localization with slip angle estimation has been evaluated in the vehicle tests in urban area of the city.

A. Sensor Specification

The test vehicles are equipped with an IMU, an GNSS receiver, and wheel speed sensors. The GNSS receiver is corrected by the RTK service, which can provide centimeter-level positioning accuracy when the fix solution is obtained. The main specification of the IMU is presented in Tab. I.

TABLE I
The Sensor Specification

Sensors	Items	Values
Gyroscopes	Bias Offset	0.1 °/s
	Bias Instability	4°/h
	ARW	$0.3^\circ/\sqrt{h}$
Accelerometers	Bias Offset	2 mg
	Bias Instability	50μg
	VRW	0.04 m/s/$\sqrt{h}$

B. Simulation

In the simulation, the true relative pitch, roll and yaw between IMU and vehicle frames are set 1°, -2°, and 2°, respectively. Different road pitch and roll angles from -20° to 20° are set to evaluate the performance of the calibration algorithm. For each road pitch and roll setup, the vehicle has 6 stationary orientation in the road plane, namely, $\psi_{br} = \{0^\circ, 30^\circ, -30^\circ, 180^\circ, -150^\circ, 150^\circ\}$. Here we use 100 times' Monte-Carlo simulation for each road attitude setup. The IMU outputs are generated from the ideal value with injected random errors. The IMU specification in the simulation is the same with one in the experiment, specified in Tab. I.

After the calibration parameters have been estimated for all the Monte Carlo trials, the root mean square errors (RMSE) of the calibration parameters are calculated. When bias offsets of accelerometers are not compensated, the RMSE of relative pitch and roll are approximately 0.12°, as shown in Fig. 4. The estimation accuracy depends on the accelerometer's bias offset, i.e., $\frac{2mg}{g}$ = 0.115°. When 90% of the offsets are compensated, we can see large improvement (over 80%) from Fig. 5. In this figure, β_x and β_y estimation results are less accurate when the road pitch/roll angles deviate from small angle assumptions. It is not obvious in Fig. 4, since accelerometers' offsets dominate the errors.

C. Experiment for IMU/Vehicle Calibration

In this experiment (Test 1), we perform "4-Orientation" calibration on the flat ground (see the zoomed sub-figure in Fig. 7). The IMU sensor output during the multi-orientation

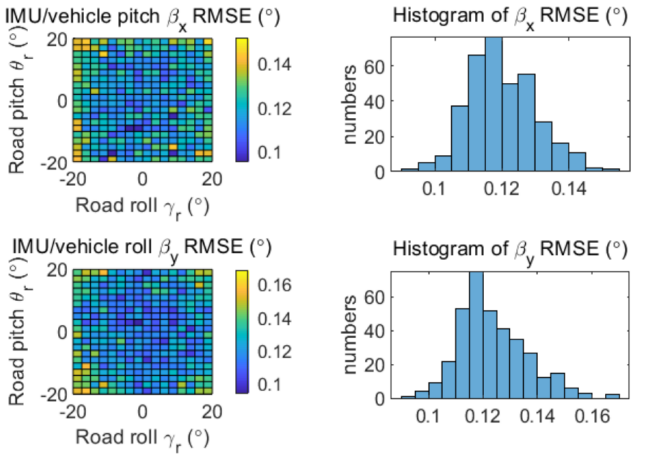

Fig. 4. IMU-Vehicle pitch/roll estimation error without compensation of accelerometers' bias.

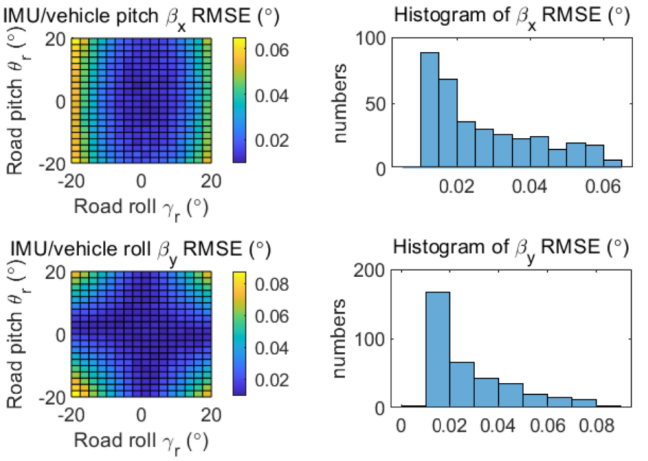

Fig. 5. IMU-Vehicle pitch/roll estimation error with 90% compensation of accelerometers' bias.

calibration is shown in Fig. 6. Each of the static intervals lasts 60s to reduce the accelerometer's noise. The 4 orientations are roughly $0°$, $180°$, $-90°$, and $90°$.

The estimation results of the relative pitch and roll are $0.469°$ and $0.747°$ (rotating from IMU-frame to vehicle frame), respectively. The estimated road pitch and roll are -0.05° and -0.07°.

The estimated relative pitch and yaw using traditional maneuver-based method are $0.434°$ and $-0.445°$, respectively, as illustrated in Fig. 8. The relative pitch is coincide with the estimation using the proposed method.

D. Road Test for Online Slip Estimation and Navigation Performance Evaluation

We have performed the integrated navigation method described in Section IV with real-world road tests.

The vehicle (different from the one in Test 1) drives normally on the urban street in mainly open sky conditions with several short ($<$10 s) RTK un-fixed periods. The total distance traveled is around 7km and the trajectory is illustrated in Fig. 9. To evaluate the performance of proposed

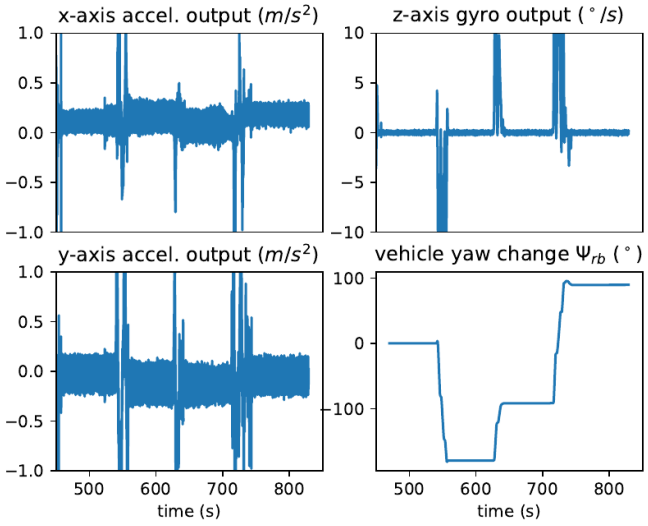

Fig. 6. IMU sensor output

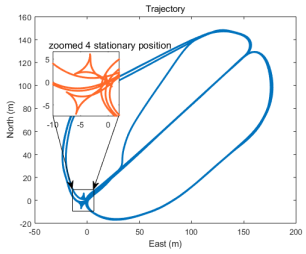

Fig. 7. Trajectory and 4 static orientations

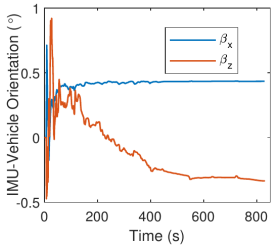

Fig. 8. IMU/Vehicle relative pitch and yaw estimation

slip calibration and compensation method, 6 GNSS signal outages are simulated by removing the GNSS updates to the Kalman filter. Each outage covers at least one turn. The ground truth is the RTK-fix solution compensated with lever-arm between the IMU and GNSS antenna. The experiments using the traditional method without slip compensation are also conducted for the comparison.

The endpoint horizontal position error of the outage and the RMSE during each outage are calculated and presented in Table II. The endpoint position accuracy of the proposed method reached 0.17%DT, which is improved 23% compared with the traditional method.

As can be seen in Fig. 9, the position of the traditional method tends to go to the inner side when the vehicle turns, even when the GNSS signal is available (see in left two subfigures). It is because there is a slip angle to the opposite direction of the turn. Our proposed method can estimate this angle and "drag" the vehicle not to "bend too much" to the turn direction. The right most subfigure presents the improved endpoint position of a GNSS outage (black markers) with proposed method. The discontinuity of red and green trajectories is the point when GNSS signal is recovered.

The state estimates of slip parameter, IMU/Vehicle misalignment, and IMU biases are illustrated in Fig. 10 and 11. The slip parameter estimation converged at 270s after several

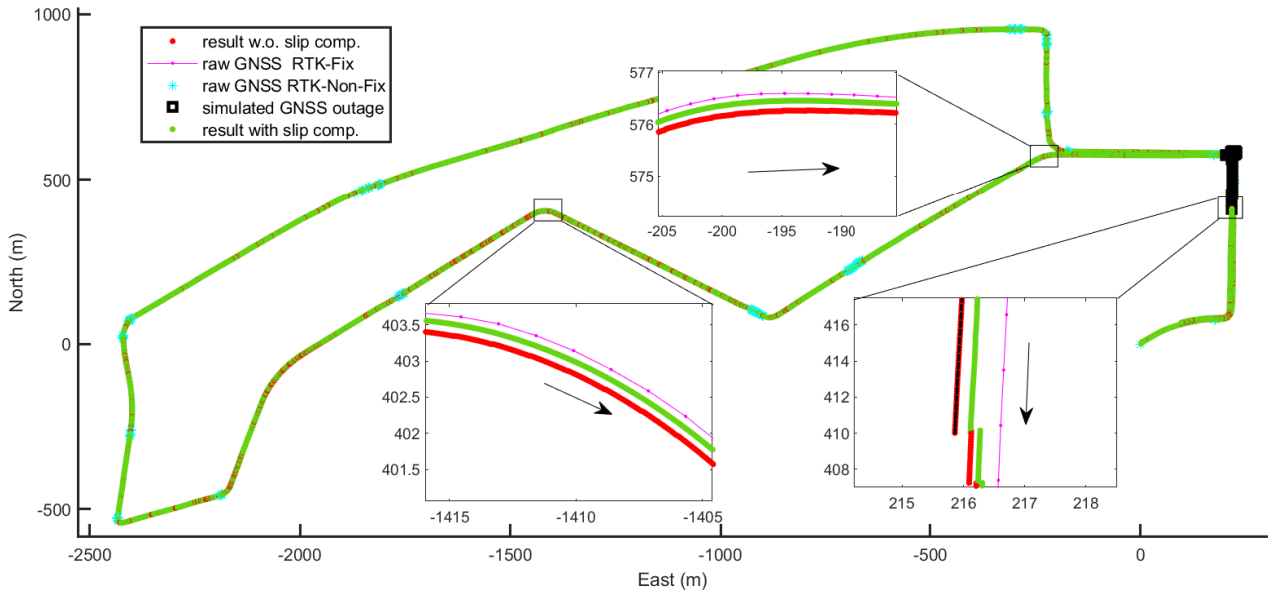

Fig. 9. The trajectory of a driving test (The black arrows are the moving directions of the vehicle. The magenta line is the RTK fix position of the antenna (with a lever-arm w.r.t IMU, i.e., [-0.12m, 0.17m, 0.868m] in right, forward, and up direction, respectively). The red trajectory is the result of traditional localization method. The green trajectory is the result of the proposed method with slip compensation. The left two zoomed subfigures show that the traditional method have a lateral position error during the turn maneuver even when the GNSS is available. The right most subfigure presents the improved endpoint position of a GNSS outage (black markers) with proposed method.)

TABLE II

GNSS OUTAGE PERFORMANCE

Test	Perform. Meas.	Traditional	Proposed
Test #1: 601.37m	Endpoint Error (m)	1.23	0.88
	RMSE (m)	1.05	0.57
Test #2: 219.27m	Endpoint Error (m)	0.82	0.57
	RMSE (m)	0.83	0.64
Test #3: 347.4m	Endpoint Error (m)	0.65	0.58
	RMSE (m)	0.40	0.38
Test #4: 589.79m	Endpoint Error (m)	0.92	0.65
	RMSE (m)	0.81	0.62
Test #5: 485.2m	Endpoint Error (m)	0.95	0.72
	RMSE (m)	0.84	0.61
Test #6: 597.83m	Endpoint Error (m)	1.24	1.05
	RMSE (m)	0.78	0.67
Average endpoint relative error (%DT)		0.22%	0.17%

turns. These state estimates also suggest the effectiveness of the proposed method.

VI. CONCLUSIONS

We have proposed a multi-orientation based IMU/vehicle relative attitude calibration method, especially the relative roll angle, which cannot be estimated in the traditional maneuver-based method. Reliable full DoF calibration can be achieved by combining our method and traditional method, which is a great benefit for the "chained calibration". To improve the localization accuracy, we have proposed an online rear-axis side-slip calibration and compensation for the integrated localization system. Real world vehicle tests have confirmed the effectiveness of proposed methods.

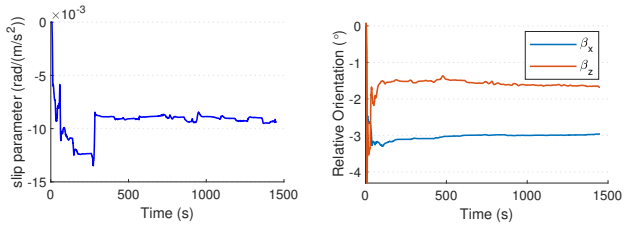

Fig. 10. The slip parameter (S) estimation (left) and misalignment(IMU/Vehicle pitch and yaw) estimation (right)

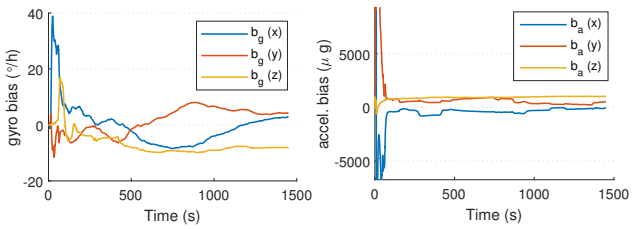

Fig. 11. IMU gyro bias estimation (left) and IMU acccelerometer bias estimation (right).

REFERENCES

[1] Y. Liu, S. Li, Q. Fu, Z. Liu, and Q. Zhou, "Analysis of kalman filter innovation-based gnss spoofing detection method for ins/gnss integrated navigation system," *IEEE Sensors Journal*, vol. 19, no. 13, pp. 5167–5178, 2019.

[2] H. Lategahn and C. Stiller, "Vision-only localization," *IEEE Transactions on Intelligent Transportation Systems*, vol. 15, no. 3, pp. 1246–1257, 2014.

[3] H. Kim, B. Liu, C. Y. Goh, S. Lee, and H. Myung, "Robust vehicle

localization using entropy-weighted particle filter-based data fusion of vertical and road intensity information for a large scale urban area," *IEEE Robotics and Automation Letters*, vol. 2, no. 3, pp. 1518–1524, 2017.

[4] G. Wan, X. Yang, R. Cai, H. Li, Y. Zhou, H. Wang, and S. Song, "Robust and precise vehicle localization based on multi-sensor fusion in diverse city scenes," in *2018 IEEE International Conference on Robotics and Automation (ICRA)*. IEEE, 2018, pp. 4670–4677.

[5] J. Levinson and S. Thrun, "Automatic online calibration of cameras and lasers." in *Robotics: Science and Systems*, vol. 2, 2013, p. 7.

[6] Y. Park, S. Yun, C. S. Won, K. Cho, K. Um, and S. Sim, "Calibration between color camera and 3d lidar instruments with a polygonal planar board," *Sensors*, vol. 14, no. 3, pp. 5333–5353, 2014.

[7] Z. Pusztai and L. Hajder, "Accurate calibration of lidar-camera systems using ordinary boxes," in *Proceedings of the IEEE International Conference on Computer Vision (ICCV) Workshops*, Oct 2017.

[8] F. M. Mirzaei and S. I. Roumeliotis, "A kalman filter-based algorithm for imu-camera calibration: Observability analysis and performance evaluation," *IEEE Transactions on Robotics*, vol. 24, no. 5, pp. 1143–1156, 2008.

[9] J. Kelly and G. S. Sukhatme, "Fast relative pose calibration for visual and inertial sensors," in *Experimental Robotics*. Springer, 2009, pp. 515–524.

[10] P. Furgale, J. Rehder, and R. Siegwart, "Unified temporal and spatial calibration for multi-sensor systems," in *2013 IEEE/RSJ International Conference on Intelligent Robots and Systems*. IEEE, 2013, pp. 1280–1286.

[11] C. Le Gentil, T. Vidal-Calleja, and S. Huang, "3d lidar-imu calibration based on upsampled preintegrated measurements for motion distortion correction," in *2018 IEEE International Conference on Robotics and Automation (ICRA)*, 2018, pp. 2149–2155.

[12] Z. F. Syed, P. Aggarwal, C. Goodall, X. Niu, and N. El-Sheimy, "A new multi-position calibration method for MEMS inertial navigation systems," *Measurement Science and Technology*, vol. 18, no. 7, pp. 1897–1907, may 2007.

[13] D. Tedaldi, A. Pretto, and E. Menegatti, "A robust and easy to implement method for imu calibration without external equipments," in *2014 IEEE International Conference on Robotics and Automation (ICRA)*. IEEE, 2014, pp. 3042–3049.

[14] J. Gao, "Development of a precise gps/ins/on-board vehicle sensors integrated vehicular positioning system," Ph.D. dissertation, The University of Calgary, 2007.

[15] Z. Liu, N. El-Sheimy, C. Yu, and Y. Qin, "Motion constraints and vanishing point aided land vehicle navigation," *Micromachines*, vol. 9, no. 5, p. 249, 2018.

[16] Q. Fu, Y. Liu, Z. Liu, S. Li, and B. Guan, "High-accuracy sins/ldv integration for long-distance land navigation," *IEEE/ASME Transactions on Mechatronics*, vol. 23, no. 6, pp. 2952–2962, 2018.

[17] Q. Chen, X. Niu, J. Kuang, and J. Liu, "Imu mounting angle calibration for pipeline surveying apparatus," *IEEE Transactions on Instrumentation and Measurement*, vol. 69, no. 4, pp. 1765–1774, 2019.

[18] Z. Bao, G. Lu, Y. Wang, and D. Tian, "A calibration method for misalignment angle of vehicle-mounted imu," *Procedia-Social and Behavioral Sciences*, vol. 96, pp. 1853–1860, 2013.

[19] X. Niu, S. Nassar, and N. El-Sheimy, "An accurate land-vehicle mems imu/gps navigation system using 3d auxiliary velocity updates," *Navigation*, vol. 54, no. 3, pp. 177–188, 2007.

[20] J. Ryan and D. Bevly, "Robust ground vehicle constraints for aiding stand alone ins and determining inertial sensor errors," in *Proceedings of the 2012 International Technical Meeting of The Institute of Navigation*, 2012, pp. 374–401.

[21] D. M. Bevly, J. Ryu, and J. C. Gerdes, "Integrating ins sensors with gps measurements for continuous estimation of vehicle sideslip, roll, and tire cornering stiffness," *IEEE Transactions on Intelligent Transportation Systems*, vol. 7, no. 4, pp. 483–493, 2006.

[22] D. Chindamo, B. Lenzo, and M. Gadola, "On the vehicle sideslip angle estimation: a literature review of methods, models, and innovations," *applied sciences*, vol. 8, no. 3, p. 355, 2018.

[23] H. F. Grip, L. Imsland, T. A. Johansen, J. C. Kalkkuhl, and A. Suissa, "Vehicle sideslip estimation," *IEEE control systems magazine*, vol. 29, no. 5, pp. 36–52, 2009.

[24] Y. Qin, *Inertial Navigation*, 2nd ed. Beijing, China: China Science Press, 2014.

[25] Z. Liu, "Vision sensor aided navigation for ground vehicle applications," Ph.D. dissertation, The University of Calgary, 2019.